Received: 2 April 2023 | Revised: 30 June 2023 | Accepted: 26 July 2023

IET Energy Systems Integration

DOI: 10.1049/esi2.12110

ORIGINAL RESEARCH

DC-side stability analysis of grid-tied converter with different control modes based on electrical torque analysis

Xu Zhang[1] | Yujun Li[1,2] | Jiapeng Li[1,2] | Ting Wu[3] | Songhao Yang[1] | Zhiguo Hao[1]

[1]School of Electrical Engineering, Xi'an Jiaotong University, Xi'an, China

[2]Department of Electrical Engineering, The Hong Kong Polytechnic University, Kowloon, Hong Kong

[3]School of Mechanical Engineering and Automation, Harbin Institute of Technology, Shenzhen, China

Correspondence

Yujun Li.
Email: yujunlizju@gmail.com

Funding information

National Natural Science Foundation of China, Grant/Award Numbers: 52277122, 72271068; Foundation of Shenzhen Science and Technology Committee, Grant/Award Numbers: GJHZ20210705141811036, GXWD20220811151845006

Abstract

The DC-side stability of the grid-tied converter under different control modes is fully investigated using electrical torque analysis. The small-signal model of a single converter connected to an ideal DC bus under various control modes is formulated. Accordingly, the damping and synchronising coefficient contributed by the DC network and controllers of grid-tied converter are separately accessed using the electrical torque analysis method and the stabilising conditions of the grid-tied converter operating under different control modes are further derived. The system stability mainly corresponds with DC network dynamics under constant active power control mode. On the contrary, the grid-tied converter under constant DC-link voltage control mode has no stability problem. Generally, elevating the DC-link capacitance or decreasing the droop gain can greatly improve the stability margin reserve of the VSC-HVDC links. In addition, the control gains of the classical PQ controller are proven to have limited impacts on DC-side system stability. Finally, the results of numerical simulation prove the validity of the proposed stability analysis method and the stable boundary for the grid-tied converter with different control modes.

KEYWORDS

power convertors, power grids, power system stability

1 | INTRODUCTION

With the large-scale construction and operation of renewable energy power stations, the long-distance bulk power transmission via converter-based HVDC systems gradually become popular in modern power grids [1]. The widespread application of voltage source converters (VSCs) brings convenience to the operation of HVDC systems [2] but simultaneously generates new challenges to the stability analysis. Many researchers focus on analysing the impacts of grid-tied converters on AC-side stability. For example, it is indicated that the system stability can be influenced by the interaction between phase locked loops' (PLLs') control dynamics, network dynamics and converter operating conditions [3], and inappropriately selected parameters of DC-link voltage control may lead to the different frequency oscillations of AC-side systems [4]. However, only a few articles provide analytical stabilising conditions for VSC-HVDC systems.

1.1 | Related works

When investigating the stability problem of modern power system, modal analysis is one of the classical and useful methods, which examines the system stability by calculating all the eigenvalues of the system state matrix: The studied system is always under a stable operation if and only if the real part of all calculated eigenvalues is negative. Based on modal analysis, some useful guidance can be given to the system operators by examining the overall system stability based on several critical system operating points [5]. In addition, some other methods derived from modal analysis, such as the gain array (RGA), are

applied in analysing the power system stability [6]. The dynamic model of the MMC-HVDC system is proposed in Ref. [7]. Based on modal analysis, the system dominant oscillatory modes can be identified, and their propensity to instability is quantified. Moreover, severe oscillations might be introduced to the HVDC system when DC-link voltage control parameters are selected improperly [8, 9]. Furthermore, the control effects of DC current flow controllers (CFCs) are analysed using Nyquist stability analysis and Bode diagram [10, 11], and the results indicate that the CFC integration has more impact on the DC-side dynamics of the multi-terminal DC (MTDC) links rather than on the AC-side dynamics of the MTDC system. In addition, the contribution of the DC network and DC-link control dynamics to the overall system stability is accessed in Ref. [12] based on net-damping criterion. However, modal analysis not only needs to acquire the detailed parameters of the whole system, but also relies on the complex computations, which fails to explain the instability mechanism of the overall system and map the stability boundary from the physical interpretation.

In order to overcome the shortcomings of the above analysis method, impedance-based analysis (IMA) is proposed and gradually become the mainstream stability analysis method [13]. To apply IMA in studying the modern power system stability, the research object should be divided into two series-connected sub-systems. The overall system will remain stable if the ratio between the impedances of the sub-systems satisfies the Nyquist stability criterion. The impedance expressions for the gird-connected converter are well derived in Refs. [14–16]. Resonance stability in HVDC systems is fully investigated in Refs. [14, 17], and it is indicated that power transmission distance, installed capacity of renewable energy and converter controller dynamics have a profound impact on DC-side resonances. In Ref. [18], it reveals that the stability problem might be introduced to HVDC systems with the alternation of power flow direction. In addition, a geometrical approach is proposed based on the conventional IMA method to well evaluate the small-signal synchronisation stability of grid-forming converter in Ref. [19]. Although the system stability can be judged only with the information of impedance using the IMA method, the proper separation of two sub-systems limits its application in complex multi-terminal HVDC systems. Furthermore, it still fails to provide analytical and concise stabilising conditions via this method.

Recently, some other novel methods are proposed for system stability assessment. Based on the graph theory, the stability of converter-tied DC system considering system structure and parameter uncertainties can be well studied, however, due to the ignorance of the interactions of the sub-systems, the proposed stability criterion may be rather conservative [20]. Furthermore, [21] proposes a stage-by-stage stability analysis method to identify which converters are mainly responsible for the overall instability, though it requires the whole system to be separated into multiple stages and fails to provide analytical stabilising conditions. The Routh Judgement applied in small-signal stability in Refs. [22, 23] assess the DC-side stability using dominant frequency analysis. Both of them find the critical variables, which have a significant impact on the stable operation of VSC-HVDC links. But only low-order power system stability can be well studied through these methods, and it is unable to provide an analytical criterion for the complex high-order system.

1.2 | Main contributions

Most existing methods are based on modal analysis or Nyquist mapping to analyse the system stability. It is difficult to obtain concise stabilising conditions using these methods, which rely on complicated mathematical modelling, complex numerical calculations and drawing quantities of the Nyquist curve. Hence, the electrical torque analysis method [24] is utilised to derive the analytical stabilising conditions for VSC-HVDC links, which provide simple and efficient small-signal stability assessment for high-order power systems without complex mathematical modelling, complicated numerical calculations and Nyquist plots. In this study, the dynamics of the grid-tied converter are firstly investigated, and the small-signal model of a single converter connected to an ideal DC bus via DC cables is formulated. Based on electrical torque analysis, the damping and synchronising coefficients contributed by DC network dynamics and VSC controllers' dynamics can be well evaluated separately. Hence, the DC-side stability of the VSC-HVDC system under different control modes can be well investigated as per the derived damping coefficient. The system stability is mainly related to the DC network dynamics under constant active power control mode, while the studied system has no stability problem under constant DC-link voltage control mode. In addition, the concise and analytical tuning rules of the power-voltage droop controller and the reactive power compensator are further proposed to improve the system stability margin, which may provide useful guidance for the control design and equipment selection.

2 | MODELLING OF GRID-TIED CONVERTER

As illustrated by Figure 1, the VSC-HVDC system to be investigated in this study consists of a two-level VSC connected to an ideal DC bus via DC cables. The DC cables adopt the classical RL model, which is sufficiently accurate for the small-signal stability analysis since the DC-side electrical oscillation frequencies do not exceed the feasible frequency band of the RL line model [11, 25]. U_{ac} is the voltage of the converter-tied AC system. U_{dc}^{r} denotes the ideal DC bus voltage, and U_{dc}^{s} represents the DC voltage at the terminal of grid-tied converter. I_{dc} is the current flowing through the DC cables, and the transmitted active power in the overall system is noted as P_t.

Furthermore, it is interesting to mention that, due to its less switch frequency, less power losses and higher reliability, more engineers prefer to choose the modular multilevel converters (MMCs). However, except that the electrical parameters

of two types of converters are different, the topology of two-level VSC is almost the same as the standard average value models of MMC [22, 23, 26]. Therefore, in order not to lose the generality, the two-level VSC is selected as the research object for the appropriate analytical model formulation and small-signal stability analysis.

2.1 | Network dynamics of grid-tied converter

The topology of the grid-tied converter is illustrated by Figure 2. I_{ac} represents the current flowing through the AC transmission line. U_c denotes the AC voltage at the terminal of grid-tied converter. R_{ac} and L_{ac} are the equivalent resistance and inductance of the converter-tied AC system,respectively. In addition, the grid-tied converter usually operates under the unit power factor control mode to take full advantage of its active power transfer capability. It is indicated that the *q-axis* current is regulated to zero, and only *d-axis* equations are taken into consideration. Therefore, the network dynamic equation in the conventional *dq* coordinate system can be written as follows.

$$U_{ac}^{d} - U_{c}^{d} = L_{ac}\frac{dI_{ac}^{d}}{dt} + R_{ac}I_{ac}^{d} - \omega_{ac}L_{ac}I_{ac}^{q} \tag{1}$$

where the superscript d and q separately denote the *d-axis* and *q-axis* component of one certain variable. ω_{ac} is the angular speed of the converter-tied AC system.

In order to establish the relationship between the converter-tied AC system and converter-tied DC system, the power balance equations must be considered. Since the grid-tied converter utilises the unit power factor control in this study, the direction of the grid voltage phasor is consistent with the direction of the selected *d-axis*. In other words, the reactive power balance can be neglected. Furthermore, the active power loss generated by the electrical equipment during the operation of the VSC-HVDC system is very small. Hence, the following equation can be held below.

$$P_t = P_{ac} = 1.5U_{ac}^{d}I_{ac}^{d} \approx P_{dc} = U_{dc}^{s}(-I_d) \tag{2}$$

where P_{ac} and P_{dc} separately represent the transmitted active power in the converter-tied AC system and converter-tied DC system. I_d denotes the DC current contributed by controllers, which will be derived in the next section.

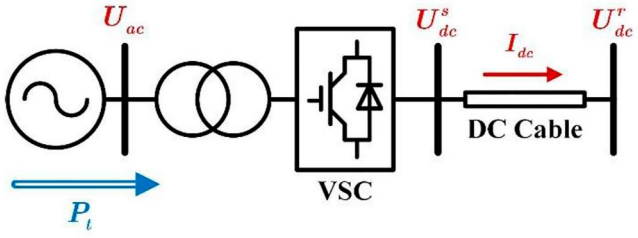

FIGURE 1 Scheme of a single converter connected to an ideal DC bus.

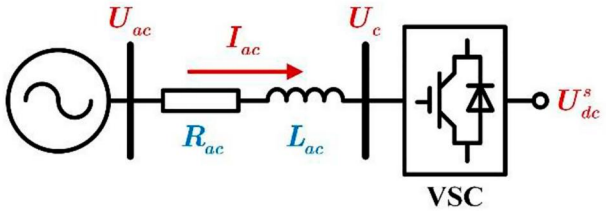

FIGURE 2 Topology of the grid-tied converter.

2.2 | Control dynamics of grid-tied converter

Since the DC-side stability of the grid-tied converter is the focus of this paper, the renewable energy generations are regarded as an ideal AC voltage source, and the phase locked loop (PLL) dynamics are neglected so that the influence of the interaction between network dynamics and controller dynamics on DC-side stability can be thoroughly discussed in the following deduction [11, 21].

For the conventional PV systems or wind power generation systems, PQ controllers are widely used, and the whole control system operates in the *dq* frame [26], which is shown in Figure 3. The current flowing through the converter-tied AC system can be well limited to its threshold value by the adopting inner current control strategy. Since the grid-tied converter operates under the unit power factor control mode, only *d-axis* dynamics of the controllers are considered. Hence, the inner current control can be depicted as follows.

$$\begin{cases} dx_c/dt = K_I^C\left(I_{ac}^{dref} - I_{ac}^{d}\right) \\ U_{ac}^{d} - U_{c}^{d} = K_P^C\left(I_{ac}^{dref} - I_{ac}^{d}\right) + x_c - \omega_{ac}L_{ac}I_{ac}^{q} \end{cases} \tag{3}$$

where x_c is the state variable associated with the integrator. K_P^C and K_I^C are the proportional and integral gain of the inner current control, respectively. I_{ac}^{dref} is the threshold value of the *d-axis* component of the current flowing through the converter-tied AC system.

In addition, the outer power control usually utilises the transmitted active power to generate and regulate the current reference so that the inner current control loop can track the value, which yields

$$\begin{cases} dx_p/dt = K_I^V\left(P_t^{ref} - P_t\right) \\ I_{ac}^{dref} = K_P^V\left(P_t^{ref} - P_t\right) + x_p \end{cases} \tag{4}$$

where K_P^V and K_I^V are the proportional and integral gain of the outer power control. P_t^{ref} is the selected active power reference of the grid-tied converter.

Furthermore, as for the classical master-slave control, if the only master converter suddenly stops operating, the remaining converters are incapable of maintaining the DC-link voltage, and the multi-terminal direct current (MTDC) grid will collapse. With the rapid development and wide application of MTDC systems, the power-voltage droop-based control strategy is highly recommended due to its advantage that each of the converters can make its own contribution to the overall system stability. Hence, based on the control scheme shown in Figure 4, the control model can be easily obtained.

$$P_t^{ref} = K_V\left(U_{dc}^s - U_{dc}^{sref}\right) + P_n \tag{5}$$

where P_n is the transmitted active power reference of the overall system. U_{dc}^{sref} denotes the DC-link voltage reference of the grid-tied converter. K_V is the droop gain of the power-voltage droop-based controller.

2.3 | Small-signal model of grid-tied converter

Combining Equations (1) and (3), (6) can be held around the equilibrium of the studied system.

$$\frac{\Delta I_{ac}^d(s)}{\Delta I_{ac}^{dref}(s)} = \frac{sK_P^C + K_I^C}{s\left(sL_{ac} + K_P^C\right) + \left(sR_{ac} + K_I^C\right)} \tag{6}$$

where Δ represents a small deviation around the equivalent operating points. s denotes the complex frequency of the VSC-HVDC system.

Generally, in the actual engineering applications, the inner current control dynamics can be reduced to a simple first-order oscillator by selecting appropriate PI coefficients as follows [22]. Hence, the control model can be further simplified.

$$\frac{L_{dc}}{K_P^C} = \frac{R_{dc}}{K_I^C} = \tau_c \quad \Rightarrow \quad \frac{\Delta I_{ac}^d(s)}{\Delta I_{ac}^{dref}(s)} = \frac{1}{(1+\tau_c s)} \tag{7}$$

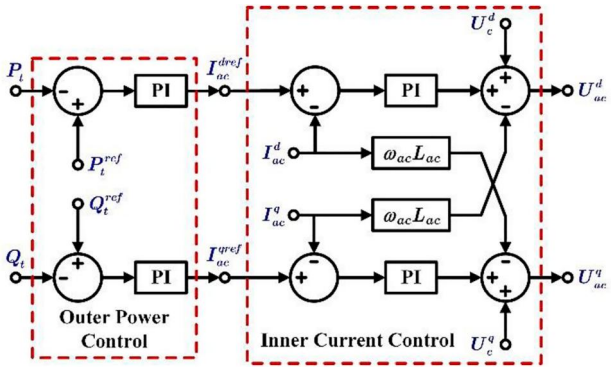

FIGURE 3 Generic control logic of conventional PQ controller.

where τ_c is the time constant of the grid-tied converter.

Linearising Equations (4) and (5) around the equilibrium of the studied system and substituting it to Equations (7), the AC current deviation influenced by various controllers can be obtained, which yields as follows

$$\Delta I_{ac}^d(s) = \frac{sK_P^V + K_I^V}{s(1+\tau_c s)}\left[K_V \Delta U_{dc}^s(s) - \Delta P_t(s)\right] \tag{8}$$

Combining Equations (2) and (8), the intermediate variables ΔP_t and ΔI_{ac}^d can be eliminated, and the DC current deviation contributed by control effects can be derived.

$$\Delta I_d(s) = \left[g_{dc} - k_u K_V B(s)\right]\Delta U_{dc}^s(s) \tag{9}$$

where g_{dc} is defined as the equivalent input conductance of the grid-tied converter and k_u is the voltage scaling factor of the studied VSC-HVDC system, which yields as follows.

$$\begin{cases} g_{dc} = \dfrac{I_{d(0)}}{U_{dc(0)}^s} = \dfrac{P_{t(0)}}{\left(U_{dc(0)}^s\right)^2}, k_u = \dfrac{3U_{ac(0)}^d}{2U_{dc(0)}^s} \\ A(s) = \dfrac{1}{1+\tau_c s}\left(K_P^V + \dfrac{K_I^V}{s}\right), B(s) = \dfrac{A(s)}{1+1.5U_{ac(0)}^d A(s)} \end{cases} \tag{10}$$

Equations (9) and (10) constitute the general small-signal model of the VSC-based converter, which provides a foundation for the following deduction and stability analysis.

3 | DC-SIDE STABILITY ANALYSIS OF A SINGLE CONVERTER CONNECTED TO AN IDEAL DC BUS

In the generic two-terminal or multi-terminal VSC-HVDC systems, the grid-tied converters may operate under different control modes to satisfy the local requirements of the power system. To fully investigate the DC-side stability of grid-tied converter under different control modes, the small-signal model of a single converter connected to an ideal DC bus is formulated, and the stabilising conditions of the overall system are also deduced based on the electrical torque method in this section.

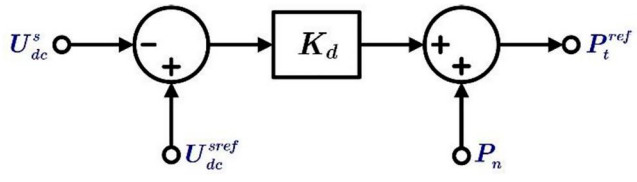

FIGURE 4 Generic control logic of power-voltage droop-based controller.

3.1 | Small-signal model of a single converter connected to an ideal DC bus

With reference to the scheme shown in Figure 1, the equivalent circuit of a single converter connected to an ideal DC bus can be illustrated by Figure 5. R_{dc} and L_{dc} separately represent the equivalent resistance and inductance of DC cables. C_{dc} denotes the DC-link capacitance installed at the terminal of the grid-tied converter. I_c is the DC current flowing through the DC-link capacitance. I_g represents the constant DC current source affected by renewable energy generations. Hence, the dynamics of the converter-tied DC system can be described by the following differential algebraic equations.

$$\begin{cases} U^s_{dc} - U^r_{dc} = R_{dc}I_{dc} + L_{dc}\dfrac{dI_{dc}}{dt} \\ I_c = C_{dc}\dfrac{dU^s_{dc}}{dt}, I_g = I_d + I_c + I_{dc} \end{cases} \tag{11}$$

Generally, appropriate input/output state variables can be used to obtain suitable *transfer functions* or *state–state expressions* for stability analysis. As for the synchronous generators (SGs) dominated power system, the power angle and angular speed are always selected as the state variables [23]. By contrast, the DC-link voltage and the DC current flowing through the DC-link capacitance are often chosen as the state variables for a clear physical interpretation in the converter-interfaced generations (CIGs) dominated power systems [22]. While, in this study, the equivalent inductance voltage noted as U_L and the DC current I_{dc} are more suitable for the electrical torque method to verify its effectiveness in the DC-side stability analysis of CIGs dominated power systems. Therefore, the inductance dynamics should be considered, which yields as follows.

$$L_{dc}\frac{dI_{dc}}{dt} = U_L \tag{12}$$

Combining Equations (11) and (12) and linearising them at the equilibrium, the *state–space expression* can be obtained.

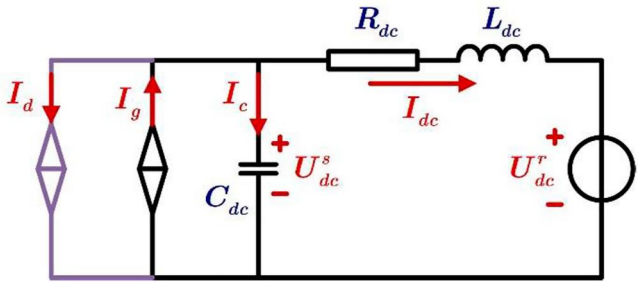

FIGURE 5 Equivalent circuit of a single converter connected to an ideal DC bus.

$$\begin{cases} L_{dc}\dfrac{d\Delta I_{dc}}{dt} = \Delta U_L \\ C_{dc}\dfrac{d\Delta U_L}{dt} = (\Delta I_g - \Delta I_d) - \dfrac{R_{dc}C_{dc}}{L_{dc}}\Delta U_L - \Delta I_{dc} \end{cases} \tag{13}$$

In addition, based on the above small-signal model, the following transfer function can be derived, which yields

$$\frac{\Delta I_{dc}(s)}{\Delta I_g(s) - \Delta I_d(s)} = \frac{1}{L_{dc}C_{dc}s^2 + R_{dc}C_{dc}s + 1} \tag{14}$$

The second-order denominator of the above transfer function corresponds to the system dominant oscillation mode. Hence, after ignoring the converter control effects, the oscillation frequency of the studied power system can be approximated as follows.

$$\omega_{dc} \approx \frac{1}{\sqrt{L_{dc}C_{dc}}} \tag{15}$$

Equations (9), (13) and (15) constitute the small-signal model of a single converter connected to an ideal DC bus. Based on the derived model, the stabilising conditions can be obtained using the electrical torque analysis method.

3.2 | Stable equilibrium points computation

As for the general power system, the system dynamics can be depicted by the following equation, which yields [27],

$$\dot{x} = f(x), x \in R \Rightarrow f(x_e) = 0 \tag{16}$$

where, f is the system equations. x represents a vector of system operating states, and x_e is the equilibrium states of the power system.

Generally, the stable equilibrium points (SEPs) can be computed by utilising algebraic solvers when an initial point sufficient close to the SEP is provided, and one common solver used for SEP computation is the Newton–Raphson (NR) method, which yields,

$$x_{i+1} = x_i - Df(x)^{-1}f(x) \tag{17}$$

Once the approximated iterative error is less than the predetermined iterative error, the NR method is terminated, and the SEPs can be obtained.

With the rapid development of power electronics-based power systems, various power electronic equipment is installed in the modern power system, which brings new challenges to equilibrium point computation. In Ref. [28], the steady-state model of VSC is established, and the efficient power flow algorithm for AC/MTDC links is proposed. In addition, the feasibility and applicability of Newton–Raphson method in power flow analysis and equilibrium computation

for power electronics-based power system are fully studied in several papers [29–31].

As for the power system investigated in this study, the SEPs can be directly calculated based on the steady-state model of the whole system without using the Newton–Raphson method, which involves quantities of numerical calculations. Hence, the system plant model and control model can be re-written in a steady state as follows.

System Plant Model (Steady State):

$$\begin{cases} U_{acn} - U^{d}_{c(0)} = R_{ac} I^{d}_{ac(0)} - \omega_{ac} L_{ac} I^{q}_{ac(0)} \\ U^{s}_{dc} - U_{dcn} = R_{dc} I_{dc(0)} \\ I_{c(0)} = 0, I_g - I_{d(0)} = I_{dc(0)} \\ P_{t(0)} = U_{acn} I^{d}_{ac(0)} = U^{s}_{dc(0)} \left(I_g - I_{d(0)} \right) \end{cases} \tag{18}$$

Control Model (Steady State):

$$\begin{cases} I^{d}_{ac(0)} = I^{dref}_{ac(0)}, P_{t(0)} = P^{ref}_{t(0)} \\ x_{p(0)} = I^{dref}_{ac(0)} \\ U_{acn} - U^{d}_{c(0)} = x_{c(0)} - \omega_{ac} L_{ac} I^{q}_{ac(0)} \\ P^{\text{ref}}_{t(0)} = K_V \left(U^{s}_{dc(0)} - U_{dcn} \right) + P_n \end{cases} \tag{19}$$

where the subscript (0) represents the steady-state value of a certain state variable. U_{acn} and U_{dcn} are separately the nominal voltage value of an ideal AC voltage source and ideal DC bus.

Based on Equations (18) and (19), the SEPs of the studied VSC-HVDC system can be obtained.

$$\begin{cases} U^{s}_{dc(0)} = \left[(U_{dcn} + K_V R_{dc}) + \sqrt{\Delta} \right] / 2 \\ \Delta = (U_{dcn} + K_V R_{dc})^2 + 4 R_{dc} (P_n - K_V U_{dcn}) \end{cases} \tag{20}$$

$$\begin{cases} P_{t(0)} = P^{\text{ref}}_{t(0)} = P_n + K_V \left(U^{s}_{dc(0)} - U_{dcn} \right) \\ I_{dc(0)} = I_g - I_{d(0)} = P_{t(0)} / U^{s}_{dc(0)} \\ I^{d}_{ac(0)} = I^{dref}_{ac(0)} = P_{t(0)} / U_{acn}, I^{q}_{ac(0)} = 0 \\ U^{d}_{c(0)} = U_{acn} - R_{ac} I^{d}_{ac(0)} \\ x_{c(0)} = R_{ac} I^{d}_{ac(0)}, x_{p(0)} = I^{d}_{ac(0)} \end{cases} \tag{21}$$

Hence, the derived small-signal model of the studied VSC-HVDC system is linearised around the SEPs by Equations (21), and the small-signal stability of the converter-tied DC system will be thoroughly evaluated in the next section.

3.3 | Electrical torque analysis

It is indicated by classical electrical torque analysis that the feedback torque deviation consists of two individual parts. Generally, the torque deviation component whose phasor direction is perpendicular to the direction of the power angle is defined as a damping torque, while the synchronising torque is defined as the component whose phasor direction is parallel to that of the power angle. The authors in Ref. [23] point out that although both damping torque and synchronising torque may influence the small-signal stability of the whole system, the impacts contributed by the damping torque is dominant. Hence, it is necessary to derive the concrete expression of the damping torque for stability analysis.

Based on Equations (9), (13) and (15), the transfer function model describes the dynamics of the studied VSC-HVDC system can be obtained, which is illustrated by Figure 6. Following the definitions of damping torque and synchronising torque in the SGs dominated power system in Ref. [22], the DC current deviation component perpendicular to the direction of I_{dc} is defined as a damping current, which is denoted by superscript D, and the component parallel to the direction of I_{dc} is defined as a synchronising current, which is distinguished by superscript S. $H(s)$ is the transfer function between the DC current flowing through the DC cables I_{dc} and equivalent inductance voltage U_L, which yields as follows.

$$H(s) = \left[g_{dc} - k_u K_V B(s) \right] \left(1 + \frac{R_{dc}}{s L_{dc}} \right) \tag{22}$$

Based on Equations (22) and the transfer function model shown in Figure 6, the damping coefficient noted as K_D and the synchronising coefficient marked as K_S can be obtained.

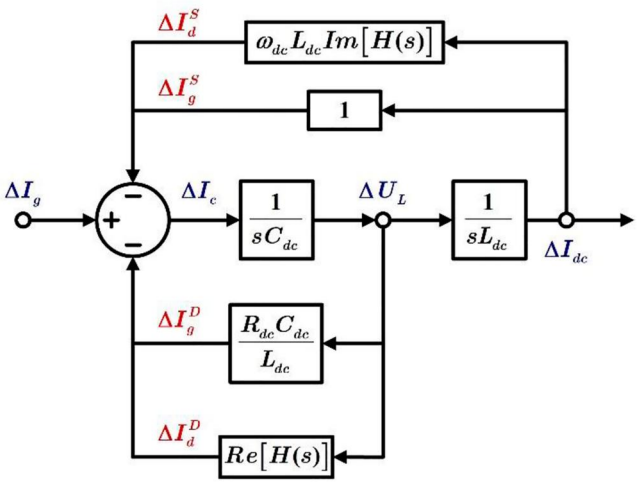

FIGURE 6 Transfer function model of a single converter connected to an ideal DC bus.

$$\begin{cases} K_D = \dfrac{R_{dc}C_{dc}}{L_{dc}} + Re[H(s)] \\ K_S = 1 + \omega_{dc}L_{dc}Im[H(s)] \end{cases} \tag{23}$$

In addition, the authors in Ref. [23] indicate that the system stability can be guaranteed when the damping coefficient is positive. Based on the stability criterion, the small-signal stability of the grid-tied converter under different control modes can be well-studied in stabilising conditions.

3.4 | Stabilising conditions under different control modes

3.4.1 | Mode 1: constant active power control:

Equation (5) reveals that when the droop gain K_V is selected as zero, the grid-tied converter operates under constant active power control mode, and the active power reference is constant. Hence, the damping coefficient of the studied VSC-HVDC system can be reduced below.

$$K_V = 0 \quad \Rightarrow \quad K_D = g_{dc} + \frac{R_{dc}C_{dc}}{L_{dc}} \tag{24}$$

Based on the electrical torque analysis, the stabilising condition under constant active power control mode can be obtained.

$$K_D > 0 \quad \Rightarrow \quad P_{t(0)} > -\frac{R_{dc}L_{dc}}{C_{dc}}\left(U^s_{dc(0)}\right)^2 \tag{25}$$

It can be easily summarised from Equation (25) that the studied system can always remain stable when the grid-tied converter works as a rectifier under constant active power control mode. On the contrary, when the grid-tied converter operates as an inverter, the network dynamics may introduce negative virtual damping to the power system. Based on Equation (25), the system stability will be destroyed once the transmitted active power exceeds the threshold, which yields as follows.

$$P^{cri}_t = \frac{R_{dc}C_{dc}}{L_{dc}}U^2_{dcn} \tag{26}$$

Due to the slight fluctuation of DC-link voltage during the normal operation of the VSC-HVDC system, the steady-state voltage value marked as $U^s_{dc(0)}$ can be replaced by the nominal voltage of the converter-tied DC system noted as U_{dcn}. P^{cri}_t is the active power transfer limit of the studied system. In addition, in the normal operation of the VSC-HVDC system, the smoothing reactors are often installed at the terminal of DC cables to suppress the DC short-circuit current. In addition, the transmission lines usually adopt a double-circuit line to guarantee the voltage stability and reduce the power loss. Hence, the equivalent resistance and inductance can be defined as follows.

$$R_{dc} = r_0 l \quad L_{dc} = l_0 l + 2L_T \tag{27}$$

where r_0 and l_0 separately denote the unit resistance and unit inductance of the DC cables. l is the power transmission distance of the studied system. L_T represents the smoothing reactor installed at the terminal of DC cables.

It is obviously indicated by Equations (26) and (27) that if the active power transfer capacity is expected to be enhanced as much as possible without destroying the system stability, and a larger DC-link capacitance should be selected, and the level of DC-link voltage should be raised.

Furthermore, considering the capacity of the grid-tied converter, the active power transfer limit of the studied system when the converter works under this control mode can be re-written below.

$$P^{cri}_t = \min\left\{P_B, \frac{r_0 l C_{dc}}{(l_0 l + 2L_T)}U^2_{dcn}\right\} \tag{28}$$

where P_B is the capacity of the grid-tied converter.

3.4.2 | Mode 2: constant DC-link voltage control:

When the grid-tied converter operates under constant DC-link voltage control mode, the DC-link voltage deviation is the same as the DC-link voltage reference deviation. Hence, the following relationship is satisfied.

$$\frac{\Delta P^{ref}_t(s)}{K_V} = 0 \quad \Rightarrow \quad K_V \to -\infty \tag{29}$$

Equation (29) reveals that the droop gain K_V needs to be regulated to one sufficient small value to ensure that the grid-tied converter operates under constant DC-link voltage control mode. Based on Equation (22), the damping coefficient affected by control dynamics will approach a relative large positive value, which reveals that the grid-tied converter under constant DC-link voltage control mode will always introduce positive virtual damping to the power system. Hence, under this circumstance, the damping coefficient will satisfy the following approximation.

$$K_D = \frac{R_{dc}C_{dc}}{L_{dc}} + Re[H(s)] \to +\infty \tag{30}$$

(30) reveals that the damping coefficient will always be positive for the grid-tied converter under constant DC-link voltage control mode, implying the system will always remain stable.

3.4.3 | Mode 3: universal droop-based control

In order to derive the stabilising conditions for the grid-tied converter under universal droop-based control mode, the

real and imaginary parts of $B(s)$ need to be separated. Hence, the transfer function $B(s)$ is re-written as follows.

$$B(s) = \frac{K_P^V s + K_I^V}{bs + a}, \begin{cases} a = 1.5U_{ac(0)}^d K_I^V - \tau_c \omega_{dc}^2 \\ b = 1 + 1.5U_{ac(0)}^d K_P^V \end{cases} \tag{31}$$

Rationalising the dominator of the expression Equation (31), the real part of the transfer function $B(s)$ can be separated out, which yields as follows,

$$Re[B(s)] = \frac{aK_I^V + bK_P^V \omega_{dc}^2}{a^2 + (b\omega_{dc})^2} \tag{32}$$

Substituting Equation (32) into Equation (23), the damping coefficient of the studied system under universal droop-based control mode can be expressed as follows.

$$K_D = g_{dc} + \frac{R_{dc}C_{dc}}{L_{dc}} - \frac{k_u K_V \left(cK_P^V + dK_I^V\right)}{a^2 + (b\omega_{dc})^2} \tag{33}$$

where

$$c = b\omega_{dc}^2 + R_{dc}a/L_{dc}, d = a - R_{dc}b/L_{dc} \tag{34}$$

Equation (33) indicates that the system stability is related to all three controllers when the grid-tied converter is under this kind of control mode. Hence, it is necessary to discuss the contribution of different controllers to the system stability.

In order to investigate the impacts of inner current control on the VSC-HVDC system stability, the sensitivity analysis of the time constant of the grid-tied converter can be carried out. Hence, by derivation of τ_c, the following expression can be held.

$$\frac{\partial K_D}{\partial \tau_c} = -\frac{k_1(a + b\omega_{dc})(a - b\omega_{dc})}{\left[a^2 + (b\omega_{dc})^2\right]} \tag{35}$$

with

$$k_1 = k_u K_V \left(K_I^V + \frac{R_{dc}K_P^V}{L_{dc}}\right) < 0 \tag{36}$$

Based on Equations (35) and (36), it can be concluded that increasing the time constant within the following range can improve the system stability.

$$\frac{1.5U_{acn}K_I^V - b\omega_{dc}}{\omega_{dc}^2} < \tau_c < \frac{1.5U_{acn}K_I^V + b\omega_{dc}}{\omega_{dc}^2} \tag{37}$$

where U_{acn} is the nominal voltage of the converter-tied AC system.

It is interesting to mention that the time constant is always selected as several milliseconds to meet the action speed of inner current control in the normal operation of the grid-tied converter. Hence, the impacts the inner current control imposed on the system stability are monotonic and limited.

In addition, since the voltage level of the converter-tied AC system is relatively high, Equation (31) can be further reduced for more detailed and concise conclusions, which yields as follows.

$$\begin{cases} a = 1.5U_{ac(0)}^d K_I^V - \tau_c \omega_{dc}^2 \approx 1.5U_{ac(0)}^d K_I^V = \overline{a} \\ b = 1.5U_{ac(0)}^d K_P^V + 1 \approx 1.5U_{ac(0)}^d K_P^V = \overline{b} \end{cases} \tag{38}$$

Substituting Equation (38) into Equation (33), the damping coefficient of the studied system can be simplified.

$$\begin{aligned} K_D &= g_{dc} + \frac{R_{dc}C_{dc}}{L_{dc}} - \frac{K_V}{U_{dc(0)}^s} \frac{\overline{a}^2 + \left(\overline{b}\omega_{dc}\right)^2}{\overline{a}^2 + \left(\overline{b}\omega_{dc}\right)^2} \\ &= g_{dc} + \frac{R_{dc}C_{dc}}{L_{dc}} - \frac{K_V}{U_{dc(0)}^s} > 0 \end{aligned} \tag{39}$$

Equation (39) indicates that the damping coefficient is hardly influenced by outer power control, which means that this kind of control also has limited impacts on the small-signal stability of the VSC-HVDC system. Thus, the dynamics of PQ controllers can be neglected when the VSC-HVDC system stability is further investigated in the future. Furthermore, it indicates that increasing the droop gain may deteriorate the system stability due to the negative value of K_V.

Substitution of Equations (10) into (39), the critical transmitted power mapping the stability boundary can be obtained.

$$P_{t(0)} > K_V U_{dc(0)}^s - \frac{R_{dc}C_{dc}}{L_{dc}} \left(U_{dc(0)}^s\right)^2 = -P_t^{cri} \tag{40}$$

Considering the minor voltage fluctuations and converter capacity limitations, the active power transfer limit under this control mode can be expressed as follows.

$$P_t^{cri} = \min\left\{P_B, -K_V U_{dcn} + \frac{r_0 l C_{dc}}{(l_0 l + 2L_T)} U_{dcn}^2\right\} \tag{41}$$

It is indicated by Equation (41) that the active power transfer limit can be greatly improved due to the negative value of the droop gain. In addition, when the droop gain is set as zero, the expression of active power transfer limit is the same as Equation (26), and when the droop gain is set as a sufficient small value, VSC controllers will no longer influence the system active power transfer capacity.

In addition, in order to better characterise the stability of the grid-tied converter, the stability margin can be defined as the relative distance between the actual transmitted active power and the calculated active power transfer limit by Equation (41), which can be expressed as follows.

$$M = 1 + \frac{P_t}{P_t^{cri}} \geq 1 - \frac{P_B}{P_t^{cri}} \tag{42}$$

It is indicated by Equation (42) that the stability margin decays with the decrease of the actual transmitted active power and reaches its minimum at $P_t = -P_B$. To ensure that the system has adequate margin under any operating points, Equation (42) should exceed a certain positive value noted as $M_{\min}$. Hence, the critical values of certain system parameters can be easily obtained.

$$\begin{cases} K_V^{\max} = \dfrac{P_B}{(M_{\min} - 1)U_{dcn}} + \dfrac{r_0 l C_{dc} U_{dcn}}{(l_0 l + 2L_T)} \\ C_{dc}^{\min} = \dfrac{(l_0 l + 2L_T)}{r_0 l U_{dcn}^2} \left(\dfrac{P_B}{1 - M_{\min}} + K_V U_{dcn} \right) \end{cases} \tag{43}$$

Based on Equation (43), the relative parameters can be optimised to guarantee the DC-side stability of the studied VSC-HVDC system even with the worst operating points.

4 | NUMERICAL SIMULATIONS

To validate the proposed stabilising conditions for the grid-tied converter under DC-side perturbations, a test VSC-HVDC system is simulated in the PSCAD/EMTDC. The transmitted active power can be regulated as a constant value or it can be changed automatically according to the universal droop-based control strategy. And the ideal DC bus is regarded as a constant DC voltage source in this case so that the mutual interaction between grid-tied converter controllers and DC networks can be thoroughly investigated. Furthermore, in order to achieve the fast-tracking property of the grid-tied converter, the time constant is set to 2 ms. The initial values of system parameters are listed in Table 1.

4.1 | Method verification

Figure 7 compares the electrical torque analysis method and the modal analysis method to verify the validity of the proposed method in DC-side stability analysis. In this case, the initial transmitted active power is set to −50 MW, and the negative sign indicates that the grid-tied converter is operating as an inverter.

Figures 7a,b depict the system dynamics under different active power perturbations. It apparently reveals that the system stability deteriorates with the decrease of the transmitted active power. Particularly, in this case, the divergent oscillation phenomenon will appear when the transmitted active power drops to −130 MW and the damping coefficient becomes a negative value of −0.0006, which well proves the feasibility of the electrical torque analysis method. It also indicates that the system stability may be compromised once the transmitted active power exceeds the critical value by Euation (41).

TABLE 1 Parameters of the test VSC-HVDC system.

Symbol	Item	Value
C_{dc}	DC-link capacitance	330 μF
L_T	Smoothing reactor	50 mH
r_0	Unit DC cable resistance	0.015 Ω/km
l_0	Unit DC cable inductance	1.635 mH/km
l	Length of DC cables	400 km
U_{dcn}	Rated DC voltage	200 kV
U_{acn}	Rated AC voltage (line to line)	220 kV
R_{ac}	Resistance of converter-tied AC system	0.016 Ω
L_{ac}	Inductance of converter-tied AC system	150 mH
K_P^C	Proportional gain of inner current control	75
K_I^C	Integral gain of inner current control	8
K_P^V	Proportional gain of outer power control	1
K_I^V	Integral gain of outer power control	10
K_V	Droop gain of power-voltage control	0
τ_c	Time constant of grid-tied converter	2 ms
S_B	Base capacity of the test system	150 MVA
SCR	Short circuit ratio of the test system	1.5

Figure 7c illustrates the root locus of the VSC-HVDC system under active power perturbations. It is apparently indicated that the dominant characteristic roots λ_1 and λ_2 gradually move towards the right half of the complex plane with the decrease of transmitted active power, which reveals that the system stability deteriorates. In contrast, the rest characteristic roots (λ_3, λ_4 and λ_5) remain the same, implying that they have little impacts on system stability. Figure 7d illustrates the variation trends of the real part of the dominant characteristic root and the damping coefficient with transmitted active power variations. It indicates that the real part of the dominant characteristic roots increases while the damping coefficient decays with the decrease of the transmitted active power. It is interesting to find that the signs of both stability indexes reverse almost at the same operating point ($P_t = 105.04$MW). The above results fully prove that the electrical torque analysis method can be utilised to judge and analyse the DC-side stability of high-order power systems without excessive model reduction and numerical calculations.

4.2 | Impacts of physical parameter variations on DC-side stability

The impacts of physical parameters on the DC-side stability are thoroughly investigated in Figure 8. Figure 8a reveals that the damping coefficient increases, and the dominant characteristic roots move towards the left half of the complex plane with the increase of C_{dc}. In contrast, promoting L_T will make

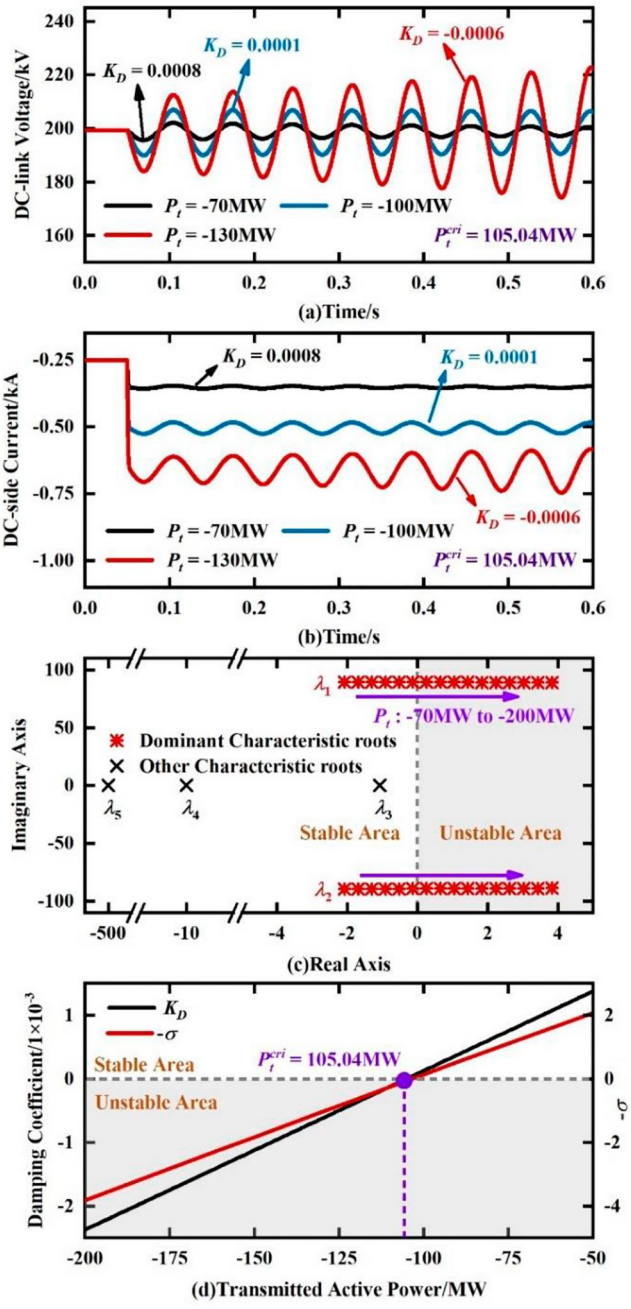

FIGURE 7 Comparison between different methods.

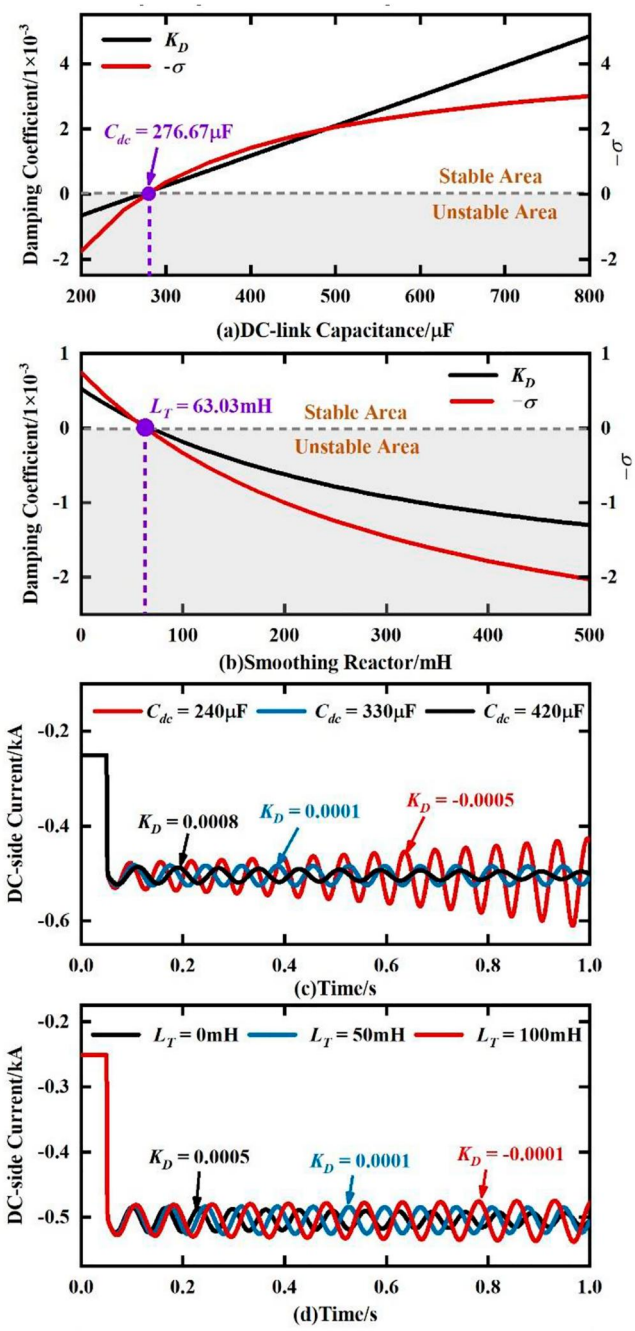

FIGURE 8 Impacts of physical parameters on DC-side stability.

the damping coefficient approaches to and eventually less than zero as shown in Figure 8b. Meanwhile, the dominant characteristic roots will move to the right half of the complex plane. The above results again verify the feasibility of the electrical torque analysis method in the DC-side stability analysis of high order power system, which has a certain application prospect. Figures 8c,d illustrate the system dynamic response with different physical parameters after a small perturbation. It is indicated by the non-linear simulation results that the system damping decays with the increase of L_T or the decrease of C_{dc}, which can be well explained by Equations (39) and (41). Once the damping coefficient becomes negative, the divergent oscillation may appear, and the system stability will be compromised. In addition, Figure 8 also reveals that C_{dc} and L_{dc} are highly related to the system oscillation frequency, which can be proved by (15). The system oscillation frequency can be reduced by elevating C_{dc} and L_T. However, in the general operation of VSC-HVDC systems, the variation range of physical parameters is not large, which indicates that the system oscillation frequency is always around 5 Hz. Hence, it is reasonable to use C_{dc} and L_{dc} to estimate the dominant oscillation frequency of the HVDC systems.

4.3 | Impacts of control parameter variations on DC-side stability

Figure 9 depicts the impacts of the bandwidth of PQ controllers on DC-side stability. The perturbation is set as the transmitted active power drop from 50 MW to 100 MW. From Figure 9a, the system is slightly improved with the increase of the time constant of inner current control, which can be proved by Equation (37). In addition, Figures 9b,c reveal that changing the proportional and integral gains of outer power control hardly influence the DC-side stability of the grid-tied converter, which can be explained by Equation (39). Hence, it is feasible to properly ignore the PQ controller dynamics when studying the small-signal stability of CIG dominated power systems, as some papers have assumed.

Figure 10 depicts the impacts of power-voltage droop-based controller on DC-side stability. Figure 10a presents the system root locus under various droop gains. With the increase of droop gain K_V, the dominant characteristic roots λ_1 and λ_2 gradually move towards the right half of the complex plane, which indicates that the system stability deteriorates. While the eigenvalue λ_5 associated with control dynamics moves in the positive direction of the real axis with the decrease of K_V. However, it is far from the imaginary axis so that the system stability will not be jeopardised. As for the rest roots, λ_3 and λ_4 remain constant with various K_V nor they can influence the stability of the overall system. In addition, as shown in Figure 10b, the damping coefficient decays with the increase of K_V, which is consistent with the trend of dominant eigenvalues, implying that the system damping gradually decreases and the system stability cannot be guaranteed. Figure 10c shows the dynamics of DC-side current with different droop gains under the same perturbation. With increase of K_V, the system stability is worsened, and the divergent oscillation will finally appear. The above results once again demonstrate the feasibility of the electrical torque analysis method in analysing the DC-side stability of CIG dominated power systems. Furthermore, the system stability can be greatly improved by selecting appropriate droop gain based on Equation (41).

4.4 | Impacts of system parameter variations on stability margin

Figure 11 illustrates the impacts of system parameters on the transmitted active power limit and stability margin. As shown in Figure 11a, the transmitted active power limit can be greatly enhanced by increasing DC-link capacitance or deceasing droop gain, which can be proved by Equation (41). In addition, Figure 11b depicts the trend of stability margin under different system parameters. When the $M_{s\ \min}$ is set to 0.2, the critical values of system parameters noted as $K_V^{\max}$ and $C_{dc}^{\min}$ can be calculated, and the results are −0.4123 and 589.06 μF. It is interesting to mention that, compared with adjusting the value DC-link capacitance, tuning the droop

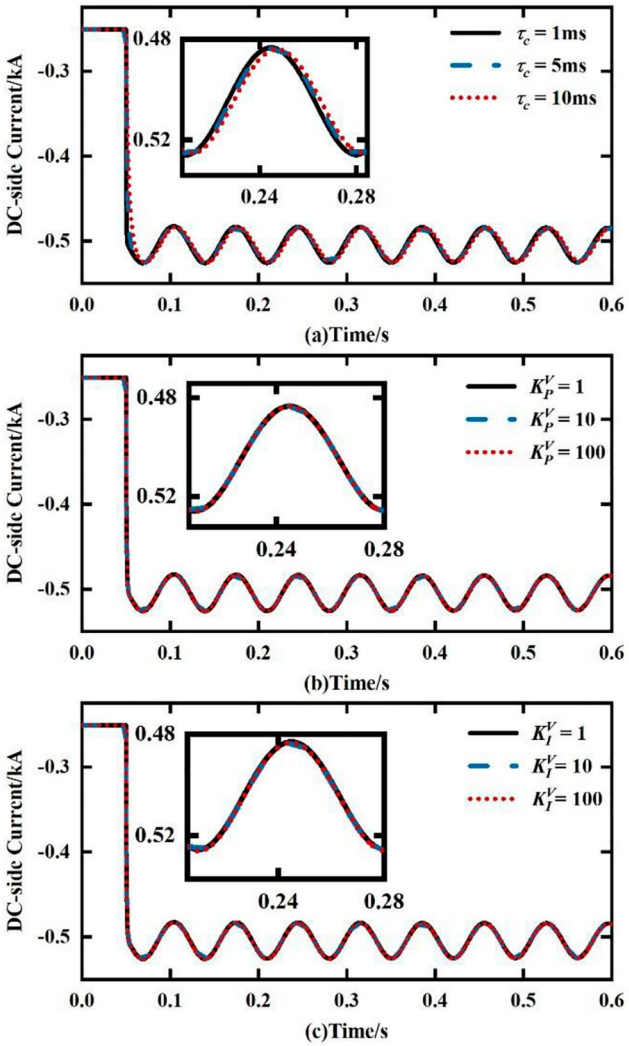

FIGURE 9 Impacts of the bandwidth of controllers on DC-side stability.

gain can better improve the system stability margin. The rest figures depict the dynamics of the studied VSC-HVDC system under the condition that the transmitted active power drops to $-P_B$. The non-linear simulations indicate that the divergent oscillations may appear once the system parameters are outside the specified range, and the whole system stability can no more be guaranteed due to the negative damping coefficient. On the contrary, when the system parameters are appropriately optimised according to Equation (43), the studied system may have sufficient stability margin and the DC-side oscillations can be well suppressed under any possible operation points.

4.5 | Impacts of AC system dynamics on DC-side stability

In order to better illustrate the impacts of AC system dynamics on DC-side stability, the related simulation results are

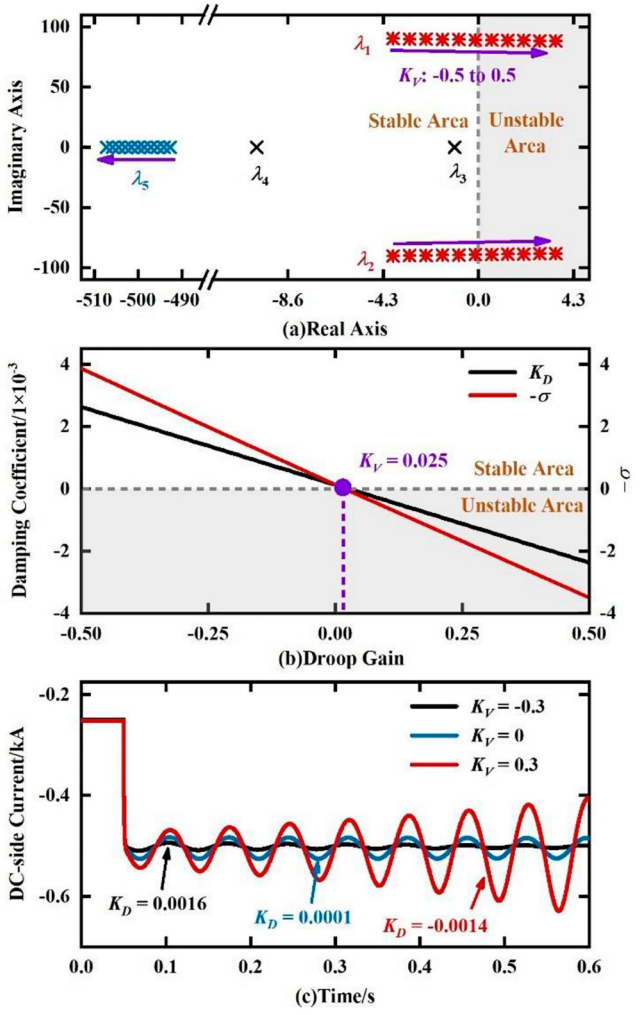

FIGURE 10 Impacts of the droop gain on DC-side stability.

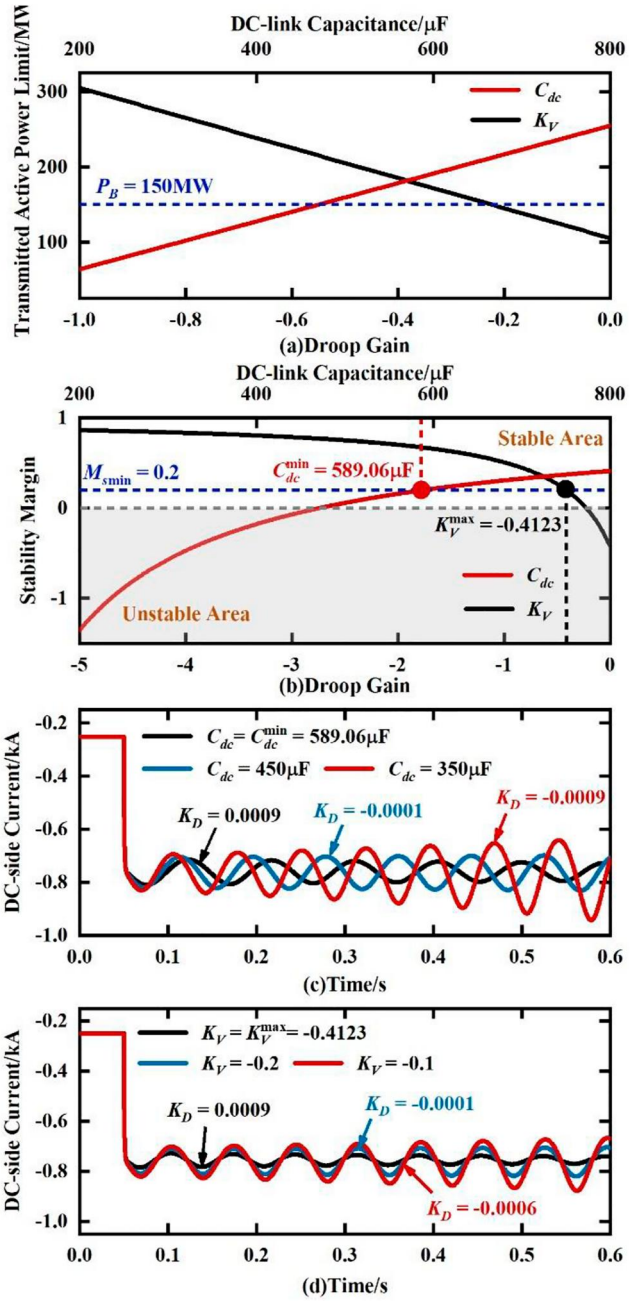

FIGURE 11 Impacts of system parameters on stability margin.

presented in this study, which is also beneficial to the explanation of the hypothesis about converter-tied AC system. As shown in Figure 12a, when the system perturbation is set as an active power fluctuation from 50 MW to 120 MW, the frequency and magnitude of DC-link current oscillation have no significant change under converter-tied AC system SCR variations. It indicates that the impacts of SCR variations on DC-side stability are minimal. This can be well explained that the strength was limited. In addition, the impacts of control gains of PLL controller on DC-side stability are described in Figure 12b,c. The simulation results reveal that the system stability always maintains with the variation of the bandwidth of the PLL controller, which indicates that the PLL dynamics also have limited impacts on DC-side stability and may not threaten the stable operation of the converter-tied DC system. Moreover, when the proportional and integral gains are selected appropriately ($K_{PPLL} = 2$, $K_{IPLL} = 400$) (see Appendix A), the related eigenvalues ($\sigma_{PLL} = -220 \pm 199j$) are far from the imaginary, which is beneficial to the system overall stability. Hence, the above control gains are used in the simulation studies.

5 | CONCLUSION AND FUTURE WORK

5.1 | Conclusion

The electrical torque analysis method is firstly applied in analysing the DC-side stability of VSC-HVDC systems considering the impacts of controllers, networks and their mutual interactions. The small-signal model of a single converter connected to an ideal DC bus is formulated and the analytical stabilising conditions of the grid-tied converter under different control modes are further deduced on the basis of the electrical torque method. Under the constant active power control mode,

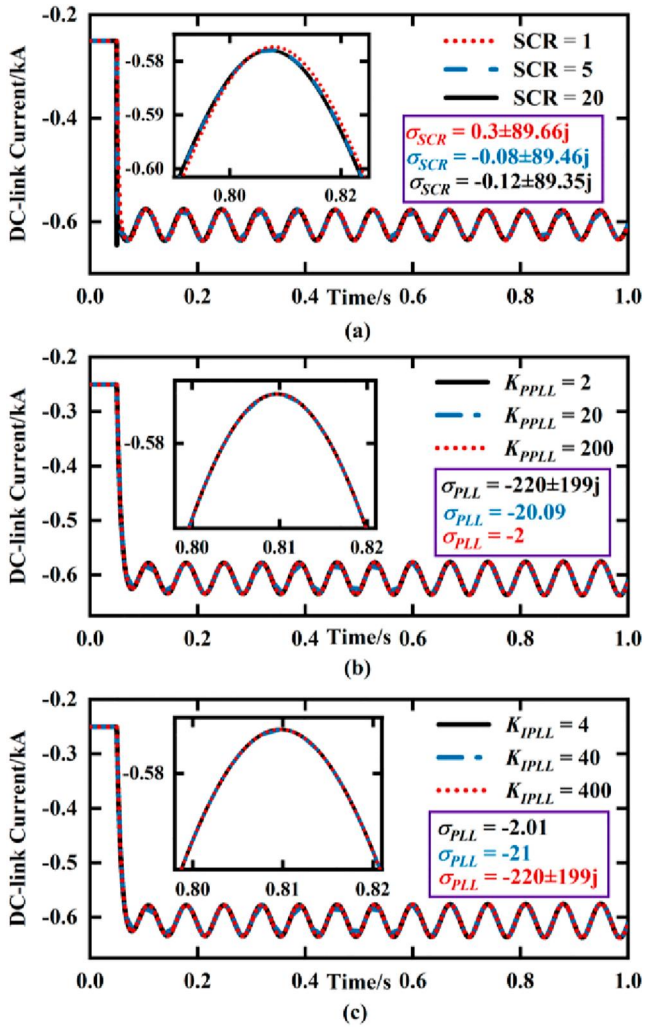

FIGURE 12 Impacts of AC system dynamics on DC-side stability.

the system stability is mainly influenced by DC network dynamics. In contrast, the system stability can be well guaranteed when the grid-tied converter is under constant DC-link voltage control mode. It is also indicated by Equation (39) that the system stability may be destroyed once the positive damping of the whole system can no more offset the negative virtual damping contributed by control dynamics. To guarantee sufficient stability margin reserve under any possible operating points, the relative system parameters can be tuned according to the principle by Equation (43). In addition, the classical PQ controllers are proven to have limited impacts on the DC-side stability. In conclusion, the electrical torque analysis method can be utilised to assess the stability of high-order power systems, which may provide some inspiration for future research on the stability analysis of multi-terminal HVDC links.

5.2 | Future work

In order to further investigate the DC-side stability of VSC-HVDC links, some more research works need to be carried out in the future, which are illustrated as follows.

A. The dynamics of the converter-tied AC system, such as SCR, PLL and AC voltage controller dynamics, have influences on system stability. In addition, the interaction between AC-side dynamics and DC-side dynamics may generate different oscillation characteristics. Hence, both of them deserve further research and comparative studies with the results in this study
B. Even though the single converter connected to an ideal DC bus under different control modes is well studied in this paper, the investigations on the stability of generic two-terminal/multi-terminal VSC-HVDC links based on the proposed method have not been completed yet. Accordingly, the grid modelling method of MTDC links will be proposed, and the feasibility and applicability of the electrical torque analysis method in a radial or meshed MTDC links can be verified in future work.

ACKNOWLEDGEMENTS

This project is supported in part by the National Natural Science Foundation of China under Grant 52277122 and 72271068, in part by the Foundation of Shenzhen Science and Technology Committee under Grant GJHZ20210705141811036 and GXWD20220811151845006.

CONFLICT OF INTEREST STATEMENT

The authors declare no conflicts of interest.

DATA AVAILABILITY STATEMENT

No data was used in the research.

ORCID

Xu Zhang https://orcid.org/0000-0003-3634-4078

REFERENCES

1. Yang, S., et al.: PLL based sub-/super-synchronous resonance damping controller for d-PMSG wind farm integrated power systems. IEEE Trans. Energy Convers. 37(4), 2370–2384 (2022). https://doi.org/10.1109/tec.2022.3174057
2. Li, Y., et al.: Synchronization stability of grid-connected VSC with limits of PLL. IEEE Trans. Power Syst. 1(1), 1–12 (2022). https://doi.org/10.1109/tpwrs.2022.3208244
3. Zhou, Y., et al.: Small-signal stability boundary of heterogeneous multi-converter power systems dominated by the phase-locked loops' dynamics. IEEE Trans. Energy Convers. 37(4), 2874–2888 (2022). https://doi.org/10.1109/tec.2022.3209628
4. Lu, D., Wang, X., Blaabjerg, F.: Impedance-based analysis of DC-link voltage dynamics in voltage source converters. IEEE Trans. Power Electron. 34(4), 3973–3985 (2019). https://doi.org/10.1109/tpel.2018.2856745
5. Song, Y., Breitholtz, C.: Nyquist stability analysis of an AC-grid connected VSC-HVDC system using a distributed parameter DC cable model. IEEE Trans. Power Deliv. 31(2), 898–907 (2016). https://doi.org/10.1109/tpwrd.2015.2501459
6. Agbemuko, A.J., et al.: Dynamic modelling and interaction analysis of multi-terminal VSC-HVDC grids through an impedance-based approach. Int. J. Electr. Power Energy Syst. 113, 874–887 (2019). https://doi.org/10.1016/j.ijepes.2019.06.029
7. Wang, Y., Zhao, C., Iravani, R.: Small signal stability investigation of the MMC-HVDC grid. IEEE Trans. Power Deliv. 37(5), 4448–4459 (2022). https://doi.org/10.1109/tpwrd.2022.3172485

8. Du, W., Fu, Q., Wang, H.: Method of open-loop modal analysis for examining the sub-synchronous interactions introduced by VSC control in an MTDC/AC system. IEEE Trans. Power Deliv. 33(2), 840–850 (2018). https://doi.org/10.1109/tpwrd.2017.2774811
9. Guan, R., et al.: Small-signal stability analysis of the interactions between voltage source converters and DC current flow controllers. IEEE Open Access J. Power Energy 7, 2–12 (2020). https://doi.org/10.1109/oajpe.2019.2930897
10. Wang, P., et al.: Nyquist stability analysis and capacitance selection for DC current flow controllers in meshed multi-terminal HVDC grids. CSEE J. Power Energy 7(1), 114–127 (2021)
11. Wang, P., et al.: Small-signal stability of DC current flow controller integrated meshed multi-terminal HVDC system. IEEE Trans. Power Syst. 38(1), 188–203 (2023). https://doi.org/10.1109/tpwrs.2022.3168023
12. Stamatious, G., Bongiorno, M.: Stability analysis of two-terminal VSC-HVDC systems using the net-damping criterion. IEEE Trans. Power Deliv. 31(4), 1748–1756 (2016). https://doi.org/10.1109/tpwrd.2016.2516987
13. Yang, D., Sun, Y.: SISO impedance-based stability analysis for system-level small-signal stability assessment of large-scale power electronics-dominated power systems. IEEE Trans. Sustain. Energy 13(1), 537–550 (2022). https://doi.org/10.1109/tste.2021.3119207
14. Xu, L., Fan, L.: Impedance-based resonance analysis in a VSC-HVDC system. IEEE Trans. Power Deliv. 28(4), 2209–2216 (2013). https://doi.org/10.1109/tpwrd.2013.2272382
15. Nian, H., et al.: Stability analysis and impedance reshaping method for DC resonance in VSCs-based power system. IEEE Trans. Energy Convers. 36(4), 3344–3354 (2021). https://doi.org/10.1109/tec.2021.3066201
16. Wu, H., Wang, X., Kocewiak, Ł.H.: Impedance-based stability analysis of voltage-controlled MMCs feeding linear AC systems. IEEE J. Emerging Sel. Top. Power Electron. 8(4), 4060–4074 (2020). https://doi.org/10.1109/jestpe.2019.2911654
17. Ji, K., et al.: DC side harmonic resonance analysis of MMC-HVDC considering wind farm integration. IEEE Trans. Power Deliv. 36(1), 254–266 (2021). https://doi.org/10.1109/tpwrd.2020.2982276
18. Amin, M., et al.: Impact of power flow direction on the stability of VSC-HVDC seen from the impedance nyquist plot. IEEE Trans. Power Electron. 32(10), 8204–8217 (2017). https://doi.org/10.1109/tpel.2016.2608278
19. Yu, J., et al.: Evaluating small-signal synchronization stability of grid-forming converter: a geometrical approach. IEEE Trans. Ind. Electron. 69(9), 9087–9098 (2022). https://doi.org/10.1109/tie.2021.3113000
20. Geng, Q., Zhou, X.: Small signal stability analysis of VSC based DC systems using graph theory. Int. J. Electr. Power Energy Syst. 137, 107830 (2022). https://doi.org/10.1016/j.ijepes.2021.107830
21. Li, Y., et al.: Small-signal stability analysis method for hybrid AC-DC systems with multiple DC buses. IEEE J. Emerging Sel. Top. Circuit Syst. 11(1), 17–27 (2021). https://doi.org/10.1109/jetcas.2020.3044091
22. Li, Y., et al.: Stability analysis of droop-based converter using SISO method from DC side perturbation. IEEE Trans. Power Deliv. 36(5), 3150–3161 (2021). https://doi.org/10.1109/tpwrd.2020.3034282
23. Li, J., et al.: Designed-oriented DC-side stability analysis of VSC-HVDC systems based on dominant frequency analysis. Int. J. Electr. Power Energy Syst., 149 (2023). to be published
24. Demello, F.P., Concordia, C.: Concepts of synchronous machine stability as affected by excitation control. IEEE Trans. Power Apparatus Syst.(4), 316–329 (1969). PAS-88. https://doi.org/10.1109/tpas.1969.292452
25. Cole, S., Beerten, J., Belmans, R.: Generalized dynamic VSC MTDC model for power system stability studies. IEEE Trans. Power Syst. 25(3), 1655–1662 (2010). https://doi.org/10.1109/tpwrs.2010.2040846
26. Beddard, A., et al.: Improved accuracy average value models of modular multilevel converters. IEEE Trans. Power Deliv. 31(5), 2260–2269 (2016). https://doi.org/10.1109/tpwrd.2016.2535410
27. Owusu-Mireku, O., Chiang, H.-D., Hin, M.: A dynamic theory-based method for computing unstable equilibrium points of power systems. IEEE Trans. Power Syst. 35(3), 1946–1955 (2020). https://doi.org/10.1109/tpwrs.2019.2946143
28. Gao, S., et al.: Efficient power flow algorithm for AC/MTDC considering complementary constraints of VSC's reactive power and AC node voltage. IEEE Trans. Power Syst. 36(3), 2481–2490 (2021). https://doi.org/10.1109/tpwrs.2020.3040356
29. Chai, R., et al.: Unified power flow algorithm based on the NR method for hybrid AC/DC grids incorporating VSCs. IEEE Trans. Power Syst. 31(6), 4310–4318 (2016). https://doi.org/10.1109/tpwrs.2015.2511303
30. Liu, Z., et al.: Further results on Newton-Raphson method in feasible power-flow for DC distribution networks. IEEE Trans. Power Deliv. 37(2), 1348–1351 (2022). https://doi.org/10.1109/tpwrd.2021.3080132
31. Miao, J., et al.: Steady-state power flow model for energy router embedded AC network and its application in optimizing power system operation. IEEE Trans. Smart Grid 9(5), 4828–4837 (2018). https://doi.org/10.1109/tsg.2017.2672821
32. Li, Y., Du, Z.: Stabilizing condition of grid-connected VSC as affected by phase locked loop (PLL). IEEE Trans. Power Deliv. 37(2), 1336–1339 (2022). https://doi.org/10.1109/tpwrd.2021.3115976

How to cite this article: Zhang, X., et al.: DC-side stability analysis of grid-tied converter with different control modes based on electrical torque analysis. IET Energy Syst. Integr. 6(1), 31–44 (2024). https://doi.org/10.1049/esi2.12110

APPENDIX A

Main parameters of the PLL

According to the authors in Ref. [32], the transfer function of the PLL can be expressed as follows.

$$s\Delta\theta(s) = \left(K_{PPLL} + \frac{K_{IPLL}}{s}\right)\Delta u_p^q(s) \qquad (A.1)$$

where u_p^q is the *q-axis* component of the voltage of the point of common coupling (PCC), and θ denotes the tracking phase angle provided by PLL. K_{PPLL} and K_{IPLL} are separately the proportional and integral gains of the PLL controller, which are configured as 2 and 400 in the simulation studies, respectively.